Molecular Neurobiology (2019) 56:6928–6940
https://doi.org/10.1007/s12035-019-1581-7

Zinc Uptake and Storage During the Formation of the Cerebral Cortex in Mice

Jessy Hasna[1] · Sylvain Bohic[2] · Sophie Lemoine[3] · Corinne Blugeon[3] · Alexandre Bouron[1,4]

Received: 17 January 2019 / Accepted: 20 March 2019 / Published online: 2 April 2019

Abstract

The cerebral cortex (or neocortex) is a brain structure formed during embryogenesis. The present study seeks to provide a detailed characterization of the Zn homeostatic mechanisms during cerebral cortex formation and development. To reach that goal, we have combined high-throughput RNA-sequencing analysis of the whole murine genome, X-ray fluorescence nanoimaging (XRF), inductively coupled plasma-atomic emission spectrometry (ICP-AES), and live-cell imaging of dissociated cortical neurons loaded with the Zn fluorescent probe FluoZin-3. The transcriptomic analysis was conducted from mRNAs isolated from cortices collected at embryonic (E) days 11 (E11), E13, and E17 and on postnatal day 1 (PN1) pups. This permitted to characterize the temporal pattern of expression of the main genes participating in the cellular transport, storage, and release of Zn during corticogenesis. It appears that cells of the immature cortex express a wide diversity of actors involved in Zn homeostasis with Zip7, SOD1, and metallothioneins being the most abundant transcripts throughout corticogenesis. The quantification of total Zn with XRF and ICP-AES reveals a reduction of Zn levels. Moreover, this is accompanied by a diminution of the size of the internal pools of mobilizable Zn. This study illustrates the tight temporal and spatial regulation of Zn homeostasis during cerebral brain development.

Keywords Brain development · Zinc · Corticogenesis · Transcriptome · RNA-seq

Introduction

The cerebral cortex, or neocortex, is a brain structure consisting of six superimposed layers of neurons, mainly of glutamatergic type. Its formation, called corticogenesis, occurs during embryogenesis and requires synchronized and regulated sequences of cell proliferation, migration, morphological differentiation, and synaptogenesis [1, 2]. At early embryonic stages, around embryonic day 9 (E9), the cortical wall mainly consists of a layer of proliferative neuroepithelial progenitor cells forming the ventricular zone and producing the first post-mitotic neurons that appear at around E10. Embryonic neurogenesis peaks at E13 and ends at ~E17 [2]. During that period, the thickness of the cortical wall increases from ~ 40 (at E11) to ~ 400 μm (at E17) [3], a tenfold enlargement that reflects an intense mitotic activity.

In the brain, the vital element zinc (Zn) is involved in a wide array of pathophysiological processes. It is for instance required for a proper brain development and formation, and many neurologic and psychiatric disorders are associated with dysregulated Zn levels. A key feature of Zn in the brain is its accumulation into synaptic vesicles of some neuronal populations [4, 5]. Thus, neuronal firing is associated with the extracellular release of this metal which is known to influence the activity of many channels and transporters [6–8]. Zn is now regarded as an endogenous and physiological modulator of synaptic transmission [8, 9]. In addition to its participation in the control of neuronal communication, Zn is reported to be an intracellular messenger controlling a wide diversity of signaling pathways. Intracellular Zn signaling can reflect its uptake and/or its release from internal stores. In neural cells

Electronic supplementary material The online version of this article (https://doi.org/10.1007/s12035-019-1581-7) contains supplementary material, which is available to authorized users.

✉ Alexandre Bouron
alexandre.bouron@cea.fr

[1] Université Grenoble Alpes, CNRS, CEA, BIG-LCBM, 38000 Grenoble, France

[2] ESRF, Grenoble, France

[3] Institut de biologie de l'Ecole normale supérieure (IBENS), Ecole Normale Supérieure, CNRS, INSERM, PSL Université Paris, 75005 Paris, France

[4] Laboratoire de Chimie et Biologie des Métaux, UMR CNRS 5249, CEA, 17 rue des Martyrs, 38054 Grenoble, France

like neurons and astrocytes, the main putative intracellular sources of mobilizable Zn are metallothioneins and mitochondria [10, 11]. The recruitment of Zn from these intracellular pools generates spatio-temporal changes in cytosolic Zn levels able to induce cell responses [4].

Despite recent progress, the molecular mechanisms governing Zn transport, storage, and release in brain cells are far from being completely characterized. This also applies to the cerebral cortex which is, together with the hippocampus, a brain structure containing high amounts of labile Zn [5]. This study was initiated to better characterize the main actors participating in Zn homeostasis during mice corticogenesis as well as their temporal expression. This is highly relevant because any alteration in Zn homeostasis is likely to alter cerebral cortex formation, and cortical abnormalities are associated with developmental neuropathologies and neurological disorders [12]. In this report, we have conducted a high-throughput RNA sequencing to assay the abundance and the developmental expression pattern of actors involved in Zn homeostasis. Total mRNAs were extracted at four time points corresponding to key periods of the cortical development: E11 (onset of corticogenesis), E13 (peak of corticogenesis), E17 (end of corticogenesis), and PN1 (beginning of the maturation of the neocortex). This was associated with measures of brain Zn contents with ICP-AES. We also determined the intracellular quantification of Zn using X-ray fluorescence (XRF) with synchrotron nanoprobe as well as the size of the main intracellular pools of mobilizable Zn in dissociated cortical neurons with live-cell fluorescent Zn imaging. Our work identified Zip7 and ZnT10 as critical actors participating in the transport of Zn during corticogenesis.

Materials and Methods

Mouse Brain Dissection and RNA Extraction

C57BL/6J mice were purchased from the Jackson's Laboratories. Since the presence of a vaginal plug is not a reliable marker of pregnancy, animals were crossed at night once a week to ease the dating of the embryos. Males were removed the morning before 9 a.m. and this day was counted as E0. Mice were killed by cervical dislocation at 11, 13, and 17 days of pregnancy. Brains of pups were collected at postnatal day 1 (PN1, first day of birth). The experimental protocol was approved by the ethical committee of the CEA's Life Sciences Division (CETEA, # A14-006).

High-Throughput Sequencing and Mapping of the Reads

From each female, one embryo or pup was decapitated and the cerebral cortex was collected for RNA sequencing. A biological sample is a cortex isolated from one embryo (or pup). Three biological samples from three different litters were collected per age. The cerebral cortices were immediately lysed for RNA extraction using the Nucleospin® RNA Kit (Macherey-Nagel) according to the manufacturer's protocol. Library preparation and Illumina sequencing were performed at the Ecole normale superieure genomic core facility (Paris, France). Messenger (polyA+) RNAs were purified from 1 μg of total RNA using oligo(dT). Libraries were prepared using the strand-specific RNA-Seq library preparation TruSeq Stranded mRNA kit (Illumina). Libraries were multiplexed by 12 on a flowcell. A 75-bp single-read sequencing was performed on a NextSeq 500 device (Illumina). A mean of 45.5 ± 8 million passing Illumina quality filter reads was obtained for each of the 12 samples. The analyses were performed using the Eoulsan pipeline [13], including read filtering, mapping, alignment filtering, read quantification, normalization, and differential analysis: Before mapping, poly N read tails were trimmed, reads ≤ 40 bases were removed, and reads with quality mean ≤ 30 were discarded. Reads were then aligned against the *Mus musculus* genome from Ensembl version 88 using STAR (version 2.5.2b) [14]. Alignments from reads matching more than once on the reference genome were removed using Java version of SAMtools [15]. To compute gene expression, *Mus musculus* GTF genome annotation version 88 from Ensembl was used. All overlapping regions between alignments and referenced exons were counted using HTSeq-count 0.5.3 [16]. The sample counts were normalized using DESeq2 1.8.1 [17]. Statistical treatments and differential analyses were also performed using DESeq2 1.8.1. The RNA-Seq gene expression data and raw fastq files are available on the GEO repository (www.ncbi.nlm.nih.gov/geo/) under accession number GSEXXX.

Determination of the Brain Zn Content

Total Zn content in embryonic and newborn murine brains was measured by inductively coupled plasma-atomic emission spectrometry (ICP-AES) using a Shimadzu ICPE-9000 spectrometer. Brains collected from animals at different ages (E11, E13, E17, and PN1) were dried on a DigiPREP block digestion system and weighed (dried weight). Dried brains were then mineralized overnight in 65% nitric acid. All samples were completed with purified water to attain a final concentration of nitric acid of 10%. A Zn standard (Sigma-Aldrich) was used for calibration. One hundred micrograms per liter of ytterbium (Sigma-Aldrich) was added to the sample and standard solutions as an internal control. Results were analyzed with the ICPE-9000 analysis software. The wavelength (206.2 nm) with the minimum interference with other elements was selected for Zn. The spectrometer gave three measurements per sample. Values with a relative standard deviation lower than 2 μg/L were retained as an indication of a

good sample mineralization. Data are expressed in ng of Zn/mg of dried brain.

Preparation of Primary Cultures of Cortical Neurons

Primary cultures of cortical neurons were prepared according to experimental procedures described in [18]. Briefly, following elimination of meninges, olfactory bulbs, and ganglionic eminences, cerebral cortices of E13 and E17 mice were isolated from five to six embryos and placed in 1 ml of an ice-cold Ca^{2+}- and Mg^{2+}-free Hank's solution supplemented with 33 mM glucose, 4.2 mM NaHCO3, 10 mM HEPES, and 1% penicillin/streptomycin. Cortical neurons were dissociated by mechanical trituration using a sterile Pasteur pipette. The cell suspension was passed through a 40-μm cell filter and isolated cells were plated at a density of ~ 1.5×10^5 cells per 16-mm-diameter glass coverslips placed into 35-mm-diameter petri dishes containing neurobasal medium supplemented with B27 (2%) and glutamine (500 μM). Cells were maintained in an incubator at 37 °C in 5% CO_2 atmosphere up to 3 days in vitro.

Zn Imaging Experiments with FluoZin-3

Changes in the free intracellular Zn concentration were recorded with the Zn fluorescent dye FluoZin-3 [19]. Imaging experiments were conducted as described previously [20, 21]. Cortical neurons were incubated with 5 μM FluoZin-3/AM for 30 min at 21–23 °C. They were then washed twice with a dye-free saline solution and kept 5 additional min in the dark. Recordings were performed with an inverted Axio Observer A1 microscope equipped with a Fluar × 40 oil immersion objective lens (Carl Zeiss, France), a DG-4 wavelength switcher (Princeton Instruments, Roper Scientific, France), and a cooled CCD camera (CoolSnap HQ2, Princeton Instruments, Roper Scientific, France). Images were captured every 5 s. The excitation light for FluoZin-3 was filtered through a 470–495-nm excitation filter and the emitted light was collected through a 525-nm filter. The baseline FluoZin-3 fluorescence was recorded for 1 min before adding FCCP or DTDP. Data acquisition and analysis were made with the MetaFluor software [20, 21]. FluoZin-3 signals were normalized to maximal signals measured in the presence of Zn/pyrithione (100%) after subtraction of the background signal obtained in the presence of TPEN [22].

Synchrotron X-ray Fluorescence Imaging

Experiments were conducted on dissociated cortical neurons collected from embryos at two time points: E13 and E17. Neurons were cultured on Si_3N_4 windows coated with poly-L-lysine and poly-L-ornithine and maintained in culture as described above. Before measurements, cells were washed with a saline solution consisting of 1.8 volume of 0.5 M Na_2HPO_4 and 1.9 volume of 0.5 M NaH_2PO_4 prior to vitrification. Experiments were carried out at the European Synchrotron Radiation Facility at the ID16A beamline. Measurements were performed at 17 keV, at liquid nitrogen temperature, on vitrified cells obtained by fast plunge-freezing in LN_2 chilled ethane (− 177 °C) using a Leica EM GP immersion freezer (Leica Microsystems, Vienna, Austria) with its environmental chamber set at 37 °C and 90% relative humidity. Cryogenic preservation allows to study neurons in their native state and preserves at best their chemical integrity [23, 24]. The position of cells was registered using an optical microscope. Frames were stored in liquid nitrogen until measurement in order to avoid cell damages. The spatial resolution was 50 nm allowing the intracellular elemental imaging.

Protein Extraction from Murine Cortices for ZnT10 and Zip7 Protein Assay by Western Blot

Isolated cortices were lysed on ice with a Ripa lysis buffer (Tris 50 mM pH 7.5, NaCl 150 mM, NP_4O 1%, NaDoC 0.5%, SDS 0.1%, EDTA 5 mM pH 8, Na_3VO_4 1 mM, NaF 10 mM and H_2O). After centrifugation at 13,000 g for 10 min at 4 °C, the supernatant was collected as the total cellular protein extracts. Protein concentration was determined using BSA range and BCA reagent (BioRad) and measured with the Tecan spectrophotometer (Infinite M 200, Tecan, Inc., USA). For Western blotting, equal amounts of protein extracts (40 μg) were separated on a 12% SDS-PAGE under a constant voltage. Proteins were then electro-transferred in Tris-Glycine buffer containing ethanol to a nitrocellulose membrane. Membranes were blocked with dry milk and then incubated overnight under stirring with appropriate primary antibodies: anti-ZnT10 antibody (Abcam, ab229954, 1/1000), anti-Zip7 antibody (ProteinTech, 19429-1-AP, 1/1000), and anti-actin antibody (Sigma, A5060, 1/1000), followed by incubation with a solution of anti-rabbit secondary antibody (Bethyl laboratories, A120-101P, 1/5000) during 45 min. Protein bands were revealed using a Fusion Fx7 apparatus (Vilbert Lourmat) and quantified using Quantity One.

Data and Statistical Analysis

For the Zn^{2+} imaging experiments, all experiments were done ≥ 5 times (e.g., with ≥ 5 distinct biological samples) using distinct dishes from three batches of cells. For the X-ray fluorescence imaging experiments, data originate from a single preparation (i.e., same batch) of primary cortical neurons culture. For each condition analyzed, elemental images of neurons were obtained from two Si_3N_4 windows. For the mRNA

and protein expression analysis, data derive from three distinct biological samples collected on three distinct embryos (or pups) that originate from three distinct females. Data are presented as means ± standard error of the mean (SEM) with n being the number of biological replicates. Differences between several groups of tissues were tested using one-way analysis of variance (ANOVA) and by means of a Student's t test when comparing two groups of cells. A p value < 0.05 was considered statistically significant. SigmaPlot (version 10.0, Systat Software) and SigmaStat (version 3.5, Systat Software) were used for plotting graphs and statistical analysis, respectively.

Results

Measurements of Total Zn Brain Content

The amount of total Zn in murine brains collected at embryonic (E) days 11, 13, and 17 (E11, E13, E17) and at postnatal day 1 (PN1) was quantified by ICP-AES. Figure 1 a shows the weight of dried brains as a function of age of the animal. A considerable brain weight gain was noted between E11 and PN1 with on average a ~ 16-fold increase. The most drastic augmentation was observed between E13 and E17 with a 4.6-fold augmentation of the brain weight whereas a 2.9- and 1.24-fold augmentation was noted between E11-E13 and E17-PN1, respectively. Measures of the amounts of Zn showed that the growth and development of the brain was associated with a parallel reduction of brain Zn levels (Fig. 1b). A sharp decrease occurred between E11 and E13, with Zn levels diminishing from 165.5 ± 22 ng/mg (E11) to 112.7 ± 4 ng/mg (E13). This decline persisted at latter stages with Zn values of ~ 95 and ~ 68 ng/mg at E17 and PN, respectively (Fig. 1b).

Measurements of Zn Concentration in Cortical Neurons

The cellular amount of total Zn was quantified in primary cultured cortical neurons dissociated at two critical time points of corticogenesis: E13 and E17, corresponding to the peak and end of bulk corticogenesis, respectively. This was achieved with high-resolution microscopic synchrotron-based chemical nanoimaging (XRF) at cryogenic temperature. In average, neurons were found embedded in a layer of amorphous ice of 20 μm as estimated through X-ray transmission measurements. Neuronal cells could still be identified using an online long-working distance optical microscope available on ID16A nanoimaging beamline. Only neuronal cell bodies were analyzed as illustrated in Fig. 2a. As reported by Colvin et al. the sulfur scan, like potassium, generally tracks the neuron mass profile and thus the cellular thickness [25]. High amounts of Zn were detected in the nuclear region but the metal was found to be present throughout the entire soma, inside and outside the nucleus as previously documented [26]. The quantitative analysis of the XRF elemental distribution shows a significant reduction of the average total Zn concentration within cortical neurons between E13 and E17 (Fig. 2b). All cells used for the Zn analysis are shown in the supplementary Figs. S1 and S2. The concentrations are classically reported as an areal mass (here in ng/mm^2) and are in the range of K and Zn concentrations found in neurons [25]. The determination of the number of Zn atoms in neuronal cell bodies was achieved by taking into account the area of each neuron imaged and used for quantification. We found in average 220 and 175 millions of Zn atoms per cell body at E13 and E17, respectively.

Intracellular Pools of Mobile Zn in Cortical Neurons

The concentration of Zn in the soma of a primary cortical neuron is in the order of 100–200 μM [26]. Only a small

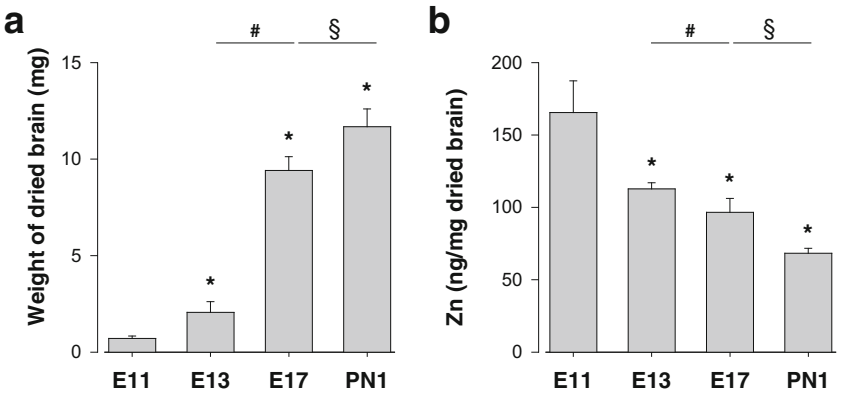

Fig. 1 Total brain Zn content during embryonic development. Brains were collected at E11 ($n = 8$), E13 ($n = 22$), E17 ($n = 8$), and on postnatal day 1 (PN1) ($n = 12$) pups. **a** The weight of the brain (dried tissue) as a function of the age of the animal. **b** The total amount of brain Zn (in ng/mg of dried brain) at each time point. Mean ± SEM, with $*p < 0.05$ when comparing vs E11, $\#p < 0.05$ when comparing E17 vs E13, and $\S p < 0.05$ when comparing PN1 vs E17 (one-way ANOVA followed by Bonferroni's test)

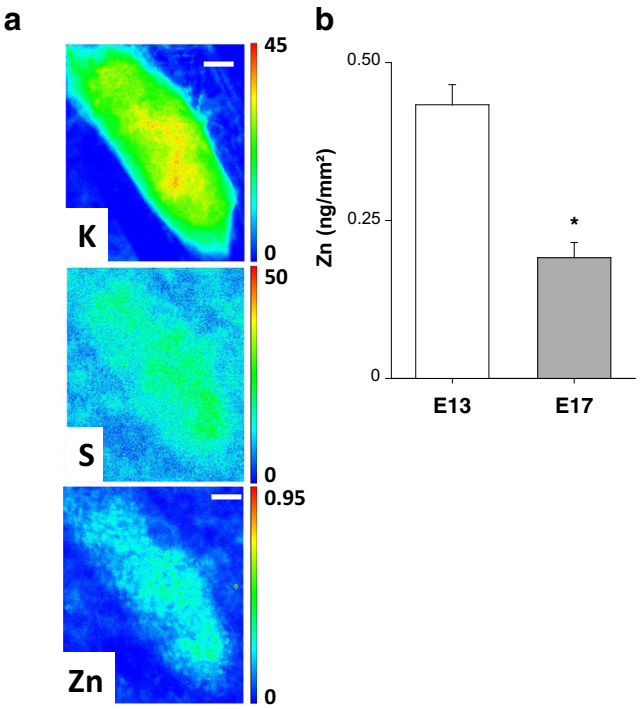

Fig. 2 Total cellular Zn content. **a** Potassium (K), sulfur (S), and zinc (Zn) concentration intensity distribution maps in a single vitrified cortical neurons from E17 mice. Nanoanalysis was performed at 120 K on frozen hydrated cortical neurons with a stepsize of 50 nm and a 50-ms dwell-time acquisition. **b** Neuronal Zn concentrations in E13 ($n = 10$) and E17 ($n = 9$) cortical neurons (colorscale bar in ng/mm^2). Mean ± SEM, with *$p < 0.05$ Student's t test. Scale bar 2 μm

fraction of this total Zn can be recruited and released from stores. Metallothioneins (MTs) and mitochondria are the most prominent pools of labile Zn in cortical neurons in culture [10, 11, 27]. The size of these pools was assessed by live-cell fluorescent microscopy on isolated cortical neurons dissociated from E13 and E17 cortices and kept up to 3 days in vitro before being loaded with the fluorescent Zn probe FluoZin-3 [19–21]. The cell-permeant and thiol-reactive oxidant DTDP (2,2′-dithiodipyridine) was employed to release Zn from MTs [10, 20, 28] whereas FCCP (carbonyl cyanide 4-(trifluoromethoxy)phenylhydrazone) was used to evoke a mitochondrial Zn release [11, 20]. The experiments were conducted as follows: DTDP (or FCCP) was applied to mobilize Zn from MTs (or mitochondria) which elevated the FluoZin-3 fluorescence [10, 11]. Then, TPEN (N,N,N′,N′-tetrakis(2-pyridylmethylethylenediamine) was added (in the absence of DTDP or FCCP) to chelate intracellular Zn ions. The exposure to TPEN rapidly diminished the intensity of FluoZin-3 signals. The maximal FluoZin-3 fluorescence was collected when superfusing cells with a TPEN-free saline supplemented with the Zn ionophore sodium pyrithione (20 μM) + Zn acetate (5 μM). This elicited a rapid elevation of the FluoZin-3 fluorescence (set at 100% after subtraction of the background signal obtained in the presence of TPEN) [22]. Figure 3 shows the changes (in %) of the FluoZin-3 fluorescence as a function of time in response to the application of DTDP (Fig. 3a) and FCCP (Fig. 3b). Whatever the embryonic age (E13 or E17), DTDP generated much larger FluoZin-3 signals than FCCP. For instance at E13, maximal DTDP- and FCCP-induced FluoZin-3 responses represented 52.7 ± 3.6% and 10.7 ± 1.2%, respectively, of the maximal FluoZin-3 signal (open circles, Fig. 3). The size of the pools of labile Zn was not influenced by the age of the cells in culture at least up to 3 days in vitro (data not shown). When similar experiments were conducted on E17 cortical neurons, DTDP and FCCP elicited FluoZin-3 signals of smaller amplitudes, representing 38.4 ± 4.9% and 4.2 ± 0.9% of the maximal FluoZin-3 signal (triangles, Fig. 3) ($p < 0.05$, Student's t test). These data indicate a reduction of the size of the DTDP- and FCCP-sensitive pools of Zn between E13 and E17.

Transcriptomic Analysis

A RNA-sequencing analysis was performed to precise the temporal expression pattern of genes involved in the cellular homeostasis of Zn. A total of 30 actors were considered, comprising genes of the ZnT and Zips families, MTs, the Zn-sensitive transcription factor MTF-1, the Zn-sensing receptor GPR39 and SOD1 (Cu/Zn superoxide dismutase 1) (Table 1). RNA abundance was presented in transcripts per million (TPM), which is more appropriate than reads per kilobase per million (RPKM) [29]. Genes having TPM value ≥ 2 are considered as actively transcribed [30]. Therefore, genes displaying TPM values < 2 were excluded from this analysis.

Zn Transporters of the ZnT Family

These actors decrease cytosolic Zn levels by accumulating Zn into organelles and/or exporting the metal out of cells [31–33]. Among the 10 ZnT genes analyzed (ZnT1-ZnT10), 3 were not expressed (TPM values < 2): ZnT2, ZnT3, and ZnT8. The most abundant transcripts of this group were ZnT1, ZnT4, ZnT9, and ZnT10 (Fig. 4a). The bar graph shown in Fig. 4b reports the changes (on a Log_2 basis) of the mRNA abundance from the most induced to the most repressed genes when compared to E11. ZnT10 was the most positively regulated gene with a 4-fold increase of its TPM values at E13 ($p < 0.001$). ZnT10 mRNA abundance then declined and remained stable until PN1 (Fig. 4b). The temporal expression profile of the ZnT4 and ZnT9 genes was different with a clear augmentation of their mRNA abundance at the end of corticogenesis (E17, PN1). The ZnT1 gene did not seem to be developmentally regulated whereas the mRNA abundance of the other genes (ZnT5–7) was stable except at PN1 where a decline was observed (Fig. 4b).

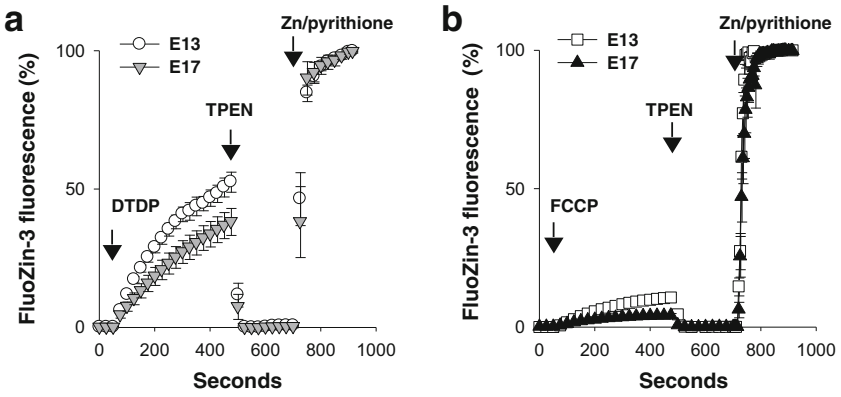

Fig. 3 Internal pools of mobilizable Zn. The size of the internal pools of Zn sensitive to DTDP (100 μM) and FCCP (1 μM) was assessed by live-cell fluorescent microscopy. Isolated cortical neurons dissociated from E13 and E17 cortices were loaded with the fluorescent Zn probe FluoZin-3. **a** and **b** The FluoZin-3 fluorescence as a function of time before and during the sequential application of DTDP (**a**) (or FCCP, **b**), TPEN (10 μM), and Zn acetate (5 μM) + Na pyrithione (20 μM). Vertical arrows indicate when substances were added. DTDP and FCCP were no longer present during the TPEN treatment. TPEN was also not present during the Zn/pyrithione challenge. FluoZin-3 signals were normalized to maximal signals obtained in the presence of Zn/pyrithione (100%) after subtraction of the background signal obtained in the presence of TPEN. Mean ± SEM. For each experimental condition, the number of cell dishes used was > 5 with $n = 167$ and 186 cells for DTDP at E13 and E17, and $n = 129$ and 172 cells for FCCP at E13 and E17, respectively. For the sake of clarity, only one point of 4 is shown

Zn Transporters of the Zip Family

Proteins of the Zip family are thought to elevate cytosolic Zn levels [31–33]. Fourteen Zip genes were analyzed (Zip1–Zip14) (Fig. 4c). Four of them were not expressed: Zip4, Zip5, Zip11, and Zip12, leaving nine Zip transcripts detected. Zip7 was by far the most expressed gene of this group with TPM values ranging from 320 to 370. Zip1, Zip3, and Zip6 were also highly expressed (Fig. 4c). Figure 4 d allows a better visualization of their temporal expression pattern. As in Fig. 4b, changes in transcripts abundance were ranked from the most augmented to the most reduced. Figure 4 d shows that Zip2 and Zip3 were the most induced genes, together with (but to a lesser extent) Zip13 and Zip6. For these latter 2 actors, a marked regulation occurred at E17. The abundance of the Zip9 and Zip14 transcripts did not vary while for all the others (Zip1, Zip7, Zip8, and Zip10), a diminution was found. Zip1 and Zip8 were severely repressed: Zip1 after E17 while the repression of Zip8 mRNAs occurred after E11 and no Zip8 mRNA could be detected at latter stages (E17 and PN1).

Metallothioneins

In the mouse, 4 MT genes are known [34] but no significant MT4 mRNA levels could be detected by this RNA-seq approach. It was thus excluded from the analysis. Transcripts of MT1–3 were found at all stages with MT1 and MT2 being the predominant MT genes at the beginning of corticogenesis (E11 and E13), and MT3 the major MT gene at the end (E17–PN1) (Fig. 5a). The expression of MT1–2 genes was transiently augmented at E13 before being repressed at E17 (Fig. 5b). For the MT3 gene, the abundance of transcripts increased from E11 to E17. Overall, MT1–3 transcripts manifested important variations during corticogenesis with distinct patterns of temporal regulation (Fig. 5b).

Transcription Factor MTF1 and GPR39, SOD1

Although the maintenance of cellular Zn homeostasis is mainly achieved by members of the Zips, ZnTs, and MTs families, additional genes were studied. They encode for MTF-1, GPR39, and SOD1 (Cu/Zn superoxide dismutase). Transcripts of the Zn-responsive transcription factor MTF-1 were detected in the developing cortex (Fig. 5c). Their abundance slightly increased throughout corticogenesis, peaking at E17. Overall, MTF-1 transcripts were not abundant when compared to the other actors analyzed above. The mRNA expression of SOD1 was also considered since this abundant protein could play a role in zinc homeostasis [35]. High mRNA levels were found throughout brain cerebral cortex development (~ 200 TPM) with a modest reduction of the SOD1 transcripts at E17 when compared to E11 (diminution of ~ 15%, $p < 0.05$). With TPM values < 0.007, the gene encoding the Zn-sensing receptor GPR39 [36] was not expressed during the formation of the murine cortex.

Top Five Genes Figure 6 is a summary graph showing the five most abundant transcripts at each age (E11, E13, E17, PN1). Three genes (Zip7, SOD1, MT2) were present in this top five list at the four time points: at the onset, at the peak, and end of corticogenesis, and also during the maturation of the cortex, indicating they play important roles in Zn homeostasis in the developing and immature cerebral cortex. Two other Zip genes were in this top 5 list: Zip1 (at E11) and Zip3 (at E17). MT3 was present from E13 to

Table 1 List of the genes analyzed

Gene name	EnsemblID	Gene description	Protein name
Mt1	ENSMUSG00000031765	Metallothionein 1	MT1
Mt2	ENSMUSG00000031762	Metallothionein 2	MT2
Mt3	ENSMUSG00000031760	Metallothionein 3	MT3
Slc30a1	ENSMUSG00000037434	Solute carrier family 30 member 1	ZnT1
Slc30a2	ENSMUSG00000028836	Solute carrier family 30, member 2	ZnT2
Slc30a3	ENSMUSG00000029151	Solute carrier family 30, member 3	ZnT3
Slc30a4	ENSMUSG00000005802	Solute carrier family 30, member 4	ZnT4
Slc30a5	ENSMUSG00000021629	Solute carrier family 30, member 5	ZnT5
Slc30a6	ENSMUSG00000024069	Solute carrier family 30, member 6	ZnT6
Slc30a7	ENSMUSG00000054414	Solute carrier family 30, member 7	ZnT7
Slc30a8	ENSMUSG00000022315	Solute carrier family 30, member 8	ZnT8
Slc30a9	ENSMUSG00000029221	Solute carrier family 30, member 9	ZnT9
Slc30a10	ENSMUSG00000026614	Solute carrier family 30, member 10	ZnT10
Slc39a1	ENSMUSG00000052310	Solute carrier family 39, member 1	Zip1
Slc39a2	ENSMUSG00000072572	Solute carrier family 39, member 2	Zip2
Slc39a3	ENSMUSG00000046822	Solute carrier family 39, member 3	Zip3
Slc39a4	ENSMUSG00000063354	Solute carrier family 39, member 4	Zip4
Slc39a5	ENSMUSG00000039878	Solute carrier family 39, member 5	Zip5
Slc39a6	ENSMUSG00000024270	Solute carrier family 39, member 6	Zip6
Slc39a7	ENSMUSG00000024327	Solute carrier family 39, member 7	Zip7
Slc39a8	ENSMUSG00000053897	Solute carrier family 39, member 8	Zip8
Slc39a9	ENSMUSG00000048833	Solute carrier family 39, member 9	Zip9
Slc39a10	ENSMUSG00000025986	Solute carrier family 39, member 10	Zip10
Slc39a11	ENSMUSG00000041654	Solute carrier family 39, member 11	Zip11
Slc39a12	ENSMUSG00000036949	Solute carrier family 39, member 12	Zip12
Slc39a13	ENSMUSG00000002105	Solute carrier family 39, member 13	Zip13
Slc39a14	ENSMUSG00000022094	Solute carrier family 39, member 14	Zip14
Mtf1	ENSMUSG00000028890	Metal response element binding transcription factor 1	MTF-1
Gpr39	ENSMUSG00000026343	G protein-coupled receptor 39	GPR39
Sod1	ENSMUSG00000022982	Superoxide dismutase 1	SOD1

PN1 and MT1 at all ages except E17. It is interesting to note the absence of members of the ZnT family in this top 5 list of the most expressed genes.

Validation of the Transcriptomic Analysis

In this last section, gene expression was verified at the protein level. We focused our attention on 2 selected actors: Zip7, the most expressed Zn transporter gene, and ZnT10, a highly regulated gene. Their expression was verified by immunoblotting. Figure 7 a shows that Zip7 protein was found at all ages whereas ZnT10 protein expression was mainly detected at latter stages (Fig. 7b), indicating that this protein controls biological processes only at the end of corticogenesis.

Discussion

The aim of this work was to gain further insight into the mechanisms participating in the homeostasis of Zn during the formation of the murine cerebral cortex. Measurements of total Zn content showed that the Zn concentration of the immature murine brain diminished during embryogenesis. Nano-XRF imaging of isolated cortical neurons illustrates that this reduction was associated with a diminution of the total intracellular Zn content between E13 and E17 as well as a decrease of the size of the pools of Zn sensitive to DTDP and FCCP. These agents were used to assess the size of the pools of mobilizable Zn associated with MTs and mitochondria, respectively [10, 11, 20]. Thus, the quantity of Zn (total and mobilizable) was down-regulated during corticogenesis, suggesting the existence of regulatory mechanisms controlling

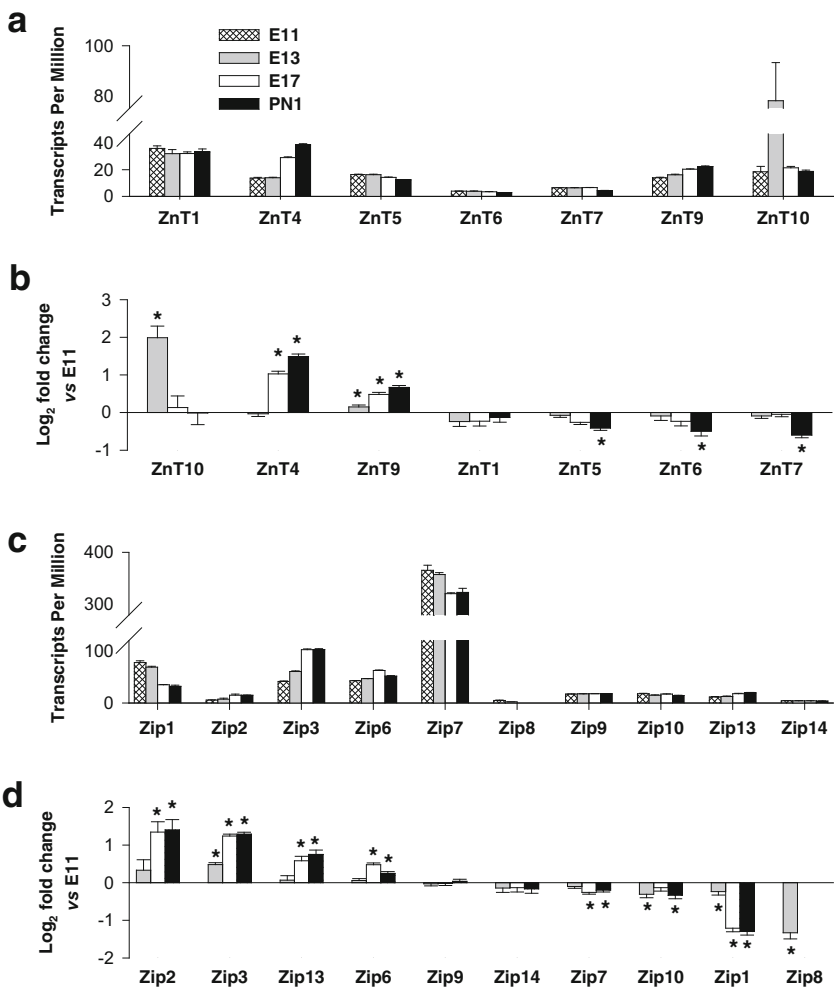

Fig. 4 Transcriptomic analysis of the ZnT and Zip transporters. The mRNA abundance of ZnTs (**a**) and Zips (**c**) is presented in transcripts per million (TPM). Only genes displaying TPM values ≥ 2 were considered [30]. **c** and **d** The changes (Log2 fold change) of the mRNA abundance of ZnTs (**b**) and Zips (**d**), from the most induced to the most repressed genes when compared to E11. Statistical treatments and differential analyses were performed using DESeq2 1.8.1 with $*p < 0.05$ when compared to E11. Mean ± SEM from $n = 3$ distinct biological samples

the uptake/efflux and storage of Zn. To further document Zn homeostasis during corticogenesis, the temporal expression pattern of genes participating in the maintenance of Zn homeostasis was investigated using a RNA-seq strategy. Two important groups of cellular Zn transporters are known: ZnTs (Zn transporters) and Zips (Zrt- and Irt-like proteins). Zips seem to mediate the uptake and/or intracellular release of Zn whereas ZnTs work in an opposite manner, contributing to the accumulation and/or efflux of Zn [31–33].

Zn Transporters of the ZnT Family

ZnT1, mainly found at the plasma membrane, was the most expressed ZnT gene but it was not developmentally regulated. The other ZnT members are predominantly found intracellularly, mostly in membranes of secretory vesicles, endosomes, and Golgi apparatus [31]. ZnT10 can also translocate to the plasma membrane and mediate an efflux of Zn [37]. ZnT1 is a ubiquitous Zn transporter counteracting elevation of intracellular Zn by ensuring its efflux out of cells. ZnT1 expression enhances markedly in the postnatal brain, particularly after P6 [38] and its brain distribution strongly correlates with synaptic Zn [38]. Deletion of the ZnT1 gene is embryonic lethal, arguing for a major role of ZnT-1 in Zn homeostasis [31, 32]. The expression of three ZnT genes was induced: ZnT4, ZnT9, and ZnT10, specifically at E13. This latter Zn transporter is present in membranes of the Golgi apparatus and translocates to the plasma membrane, allowing an efflux of Zn [37]. Immunoblots failed to detect ZnT10 proteins before E17, indicating that mRNA levels did not correlate with protein abundance. The analysis of the transcriptome and proteome during early embryonic brain development found 60–70% concordant regulation between mRNAs and their corresponding proteins, with only 20–30% showing clear opposite regulation [39].

ZnT4 and ZnT9 are two other important ZnT genes during cerebral cortex development. Both have been shown to be highly expressed in the brain, including the human brain, particularly the fetal brain [40]. These genes were up-regulated, with a marked stimulation at the end of corticogenesis. ZnT4 is mainly found in lysosomal and endosomal compartments whereas ZnT9 is an ER protein [40]. This indicates that the

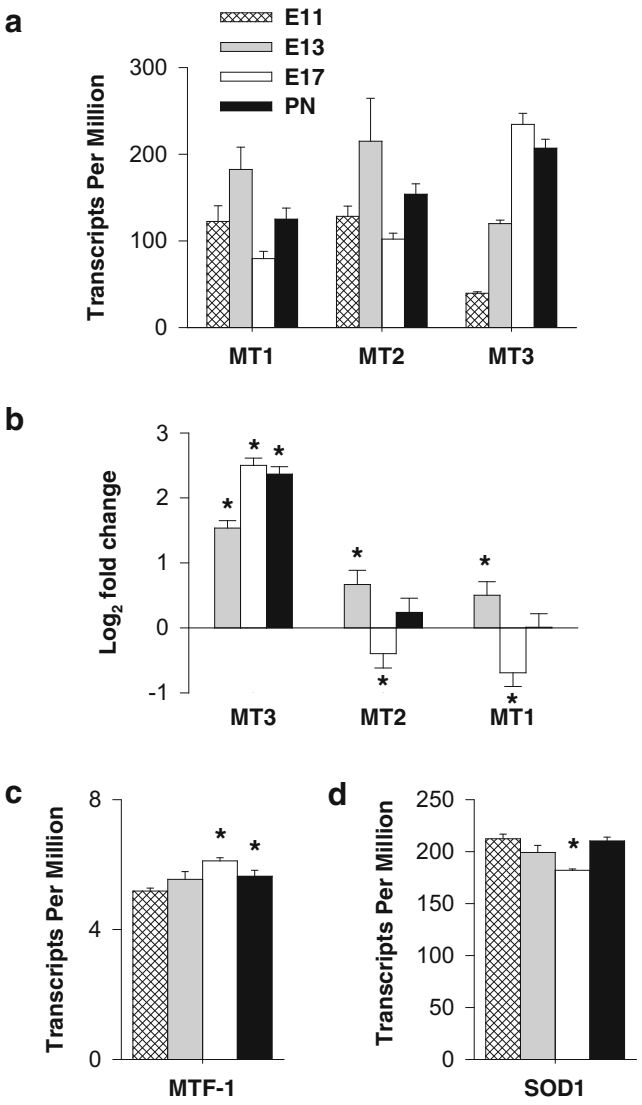

Fig. 5 Transcriptomic analysis of the MTs, MTF-1, and SOD1. **a** and **b** TPM values (**a**) and the changes (Log2 fold change) of the mRNA abundance (**b**) of MTs. The abundance of the MTF-1 and SOD1 genes are shown in **c** and **d**, respectively. Statistical treatments and differential analyses were performed using DESeq2 1.8.1 with $*p < 0.05$ when compared to E11. Mean ± SEM from $n = 3$ distinct biological samples

end of corticogenesis was accompanied by a ZnT4-dependent sequestration of Zn into endo/lysosomes and a ZnT9-dependent sequestration of Zn into the ER. Three ZnT genes were repressed: ZnT5–7. They are required for the early secretory pathway [32], controlling the uptake of Zn into vesicular compartments [31]. Low ZnT5–7 mRNA levels were found and their abundance decreased significantly at PN1, suggesting that they do not play central roles during the maturation of the cortex. Of particular interest is ZnT3, a vesicular transporter accumulating Zn into synaptic vesicles [41] involved in the formation of a histochemically (or chelatable) pool of Zn. We found no evidence for ZnT3 mRNA expression during embryogenesis, a finding consistent with a previous report showing that the embryonic mouse brain lacks such histochemically reactive pool of Zn [42]. Its size increases substantially during postnatal development particularly after PN5 [43]. Collectively, synaptic vesicular Zn seems to appear only after birth, suggesting that the formation of the embryonic cerebral cortex does not require the extracellular release of synaptic Zn. Alternatively, the failure to detect ZnT3 transcripts (and this applies to the other undetected transcripts of this study) may reflect a restricted ZnT3 gene expression in discrete cell populations.

Zn Transporters of the Zip Family

With higher TPM values, Zip transcripts (Zn influx transporters) predominate over ZnT transcripts (Zn efflux transporters). Overall, the most abundant Zip transcripts were Zip7 and, to a lower extent, Zip1, Zip3, and Zip6. These 4 genes were however differentially regulated during development. Four Zip genes were induced (Zip2, Zip3, Zip6, Zip13) and 4 Zip genes were repressed (Zip1, Zip7, Zip8, Zip10), leaving 2 genes not affected (Zip9 and Zip14) with low and stable mRNA levels throughout corticogenesis. Zip2 was the most induced gene, followed by Zip3, Zip13, and Zip6. The induction of these 4 Zip genes mainly occurred after E13, except Zip3 of which expression started to augment at E13. Zip3 expression was detected at E14 and displays a high expression in the embryonic as well as in the adult brain [44]. Data from knockout mice suggest that Zip3 plays a minor role in Zn homeostasis during mouse development, probably due to the existence of compensatory mechanisms and functional redundancy between Zip proteins [44]. In each instance, comparable amounts of mRNAs were found at E17 and PN1. The plasma membrane Zip2 transporter [32] [31] was detected at

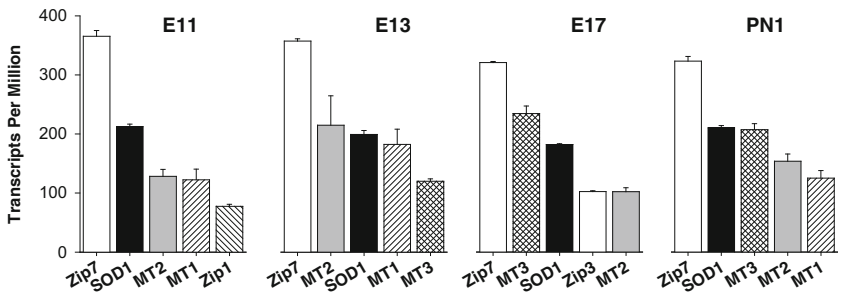

Fig. 6 Top five genes expressed during brain development. This figure shows the 5 most expressed genes at each age (E11, E13, E17, PN1). Data derived from Figs. 4 and 5

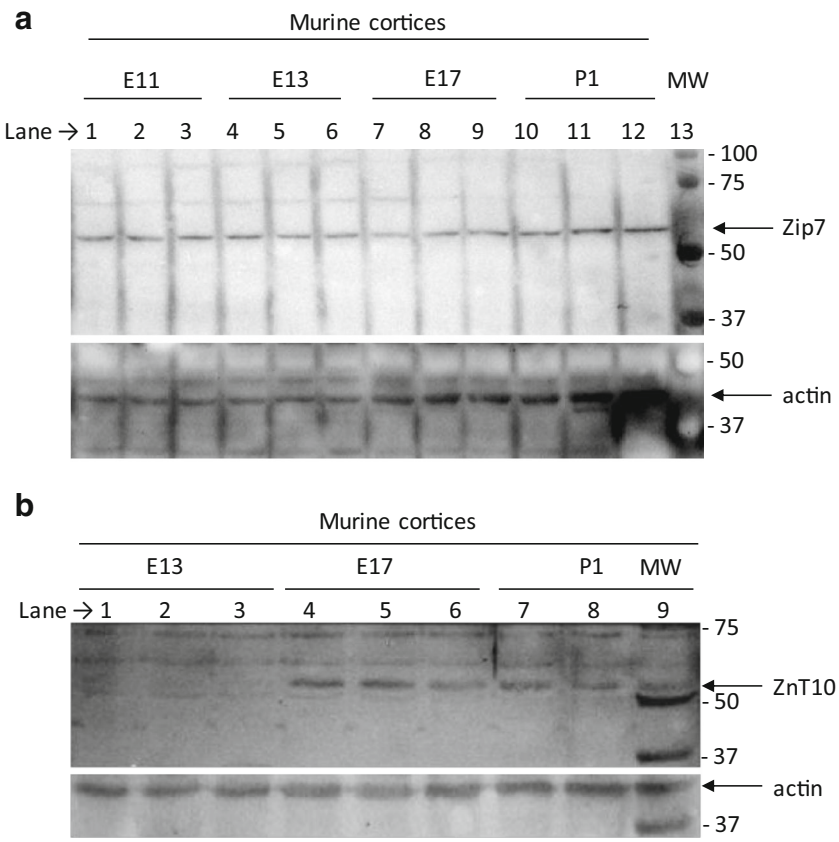

Fig. 7 Zip7 and ZnT10 protein expression. Immunoblots showing Zip7 (**a**) and ZnT10 (**b**) protein expression. Proteins were extracted from three different cerebral cortices from three distinct brain embryos (or pups) obtained from three distinct females. The age of the animal (E11, E13, E17, and PN1) is indicated above each lane. **b** Molecular weight markers have been loaded with a PN1 biological sample

low mRNA levels but it was the most positively regulated Zip gene, with a strong augmentation of its mRNA abundance at E17. This suggests that Zip2-dependent functions are mainly required at the end of corticogenesis. Moderate mRNA levels of Zip6 and Zip13 were found. Their gene expression was also induced at the end of corticogenesis. Both contribute to cytosolic Zn elevations by promoting the entry of Zn (Zip6) and its release from the Golgi (Zip13) [32] [33].

Four genes of the Zip family were repressed: Zip7, Zip10, Zip1, and Zip8. A marked repression of the Zip8 gene expression was observed at E13, a result consistent with a previous report showing a strong down-regulation during the differentiation of neural progenitor cells [45]. Zip8 protein, detected in the subventricular zone at E14, would be necessary for neural progenitor cells but not for differentiated cells [45]. Zip7 is a ubiquitously expressed ER resident protein mediating a release of Zn activating downstream multiple tyrosine kinases [46]. The Zip7 gene was the most expressed gene encoding for a Zn transporter. The Zip7 protein is already present in E14 cortical neurons, located in the membrane of the ER/Golgi [47]. A modest reduction of the Zip7 mRNA abundance was noted at E17 and PN1, suggesting important roles for the Zip7-dependent functions at early stages of corticogenesis. Zip1 was, after Zip7, the most expressed Zip gene at the beginning of corticogenesis (E11). Both were in the top five list of the most abundant transcripts at E11. This shows that at the beginning of corticogenesis, a time period where neural precursor cells predominate over post-mitotic neurons, non-neuronal cells express high mRNA levels of transporters able to elevate cytosolic Zn levels: Zip7 and Zip1. They are involved in the release and uptake of Zn, respectively. The abundance of Zip1 transcripts drastically diminished at E17. A low abundance of Zip10 mRNA was noted and it further declined at E13 and onward. Zip12 protein is highly expressed in adult mouse brain and in the developing frog brain participating in neural tube closure during frog (*Xenopus tropicalis*) embryogenesis [48]. We failed to detect Zip12 transcripts (TPM < 2), indicating that contrary to the frog brain, Zip12 is not a critical mediator of the formation and development of the mouse cerebral cortex.

In addition to ZnTs and Zips, MTs are important players regulating intracellular Zn concentration and localization. These abundant cytosolic metal-binding proteins are mainly found in the cytosol but they can translocate to the nuclei, lysosomes, or mitochondria [34]. MTs participate in the storage, distribution, and release of Zn, exerting thus a central role in Zn homeostasis. MT1–2 genes were the predominant MT genes at the beginning of corticogenesis, at stages where the cortical wall mainly harbors non-neuronal cells. MT1–2 expression increased at E13, a period of intense production of progenitor cells, and then declined at E17. Comparable mRNA levels were noted at E11 and PN1. The expression

of the MT3 gene was also highly regulated with a sharp augmentation of the MT3 mRNA levels at E17 (end of neurogenesis). The exact biological functions of MT3 are still obscure. This actor might have roles outside the maintenance of cellular Zn homeostasis, for example by controlling cytoskeletal dynamics and lysosomal functions [49]. Overall, MT1–2 and MT3 genes exhibited distinct patterns of expression.

GPR39 is a Gαq protein-coupled receptor highly specific to extracellular Zn ions. Its activation generates a phospholipase C-dependent Ca release and enhances the activity of protein kinases. GPR39 seems to serve as a metabotropic plasma membrane receptor sensing extracellular Zn and regulating diverse cellular functions [36]. We found no evidence for the expression of the GPR39 gene during the formation of the cerebral cortex. The lack of ZnT3 and GPR39 expression further supports the contention that extracellular Zn signaling is unlikely to play prominent roles during corticogenesis.

The transcription factor MTF-1 is regarded as a cellular sensor of Zn status. In response to cytosolic elevations of Zn, MTF-1 translocates to the nucleus and stimulates the expression of proteins lowering cellular Zn levels such as ZnT1 and MTs. Homozygous MTF-1$^{-/-}$ knockout embryos die during embryonic development [50], showing that MTF-1 exerts essential biological functions. The expression of the Cu/Zn superoxide dismutase (SOD1) was also considered. Indeed, it is a very abundant enzyme representing up to 2% of the total detergent-soluble proteins in mammalian cells [51]. It may thus bind significant amounts of Zn. In addition to its well-known antioxidant enzymatic function, SOD1 could also serve as a Zn supplier, at least under Zn-deficient conditions [35]. Therefore, SOD1 has been proposed to be a cytosolic sensor of Zn that could play an important role in zinc homeostasis [35]. It had the same mRNA abundance as MTs except at the onset of corticogenesis where SOD1 was, after Zip7, the most expressed gene.

Limitations of the Work

Two types of Zn transport systems through membranes were considered in this study: ZnTs and Zips. However, additional actors can deliver Zn into cells like NMDA receptors, voltage-gated Ca channels, or TRPC6 channels [52]. Their expression was however not investigated in the present study (manuscript in preparation). Another important limitation of this work is the fact that mRNA levels do not necessarily correlate with proteins levels as illustrated for ZnT10. As pointed out above, a previous transcriptomic and proteomic analysis reported 60–70% concordant regulation between mRNAs and their corresponding proteins during early embryonic brain development [39]. Another limitation that has to be mentioned is the fact that the cerebral cortex harbors various types of neural cells. For instance, at the beginning of corticogenesis, progenitor cells predominate in the cortical layer whereas post-mitotic neurons appear at latter stages. For instance, at E13 80 to 90% of the cells are Tuj1-positive (a marker of post-mitotic neurons), showing that our cell culture model is highly enriched in neurons [53]. Therefore, some non-neuronal cells may have contributed to the results obtained.

Conclusions

The aim of this work was to gain a better understanding of the Zn homeostatic mechanisms during cerebral cortex formation and development. Gene expression was investigated at the transcriptome level using a RNA-seq analysis of the whole murine genome. It permitted to characterize the temporal pattern of expression of the main genes participating in the cellular transport, storage, and release of Zn during corticogenesis. This approach was combined with quantification of total amounts of Zn with XRF and ICP-AES. Both techniques revealed a general diminution of Zn levels during brain formation. This was accompanied by a down-regulation of the size of the internal pools of mobilizable Zn assessed by live-cell fluorescence microscopy on dissociated cortical neurons. Figure 8 summarizes some of the main findings of this study. It represents the most abundant mRNAs present at E11 (onset of corticogenesis) and

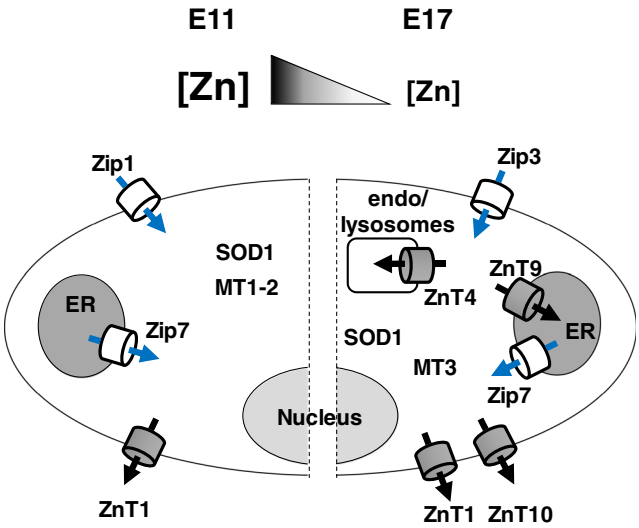

Fig. 8 Evolution of the Zn homeostatic mechanisms. This scheme summarizes some of the main results characterizing the evolution of the Zn homeostatic mechanisms between the beginning (E11) and the end of corticogenesis (E17). A reduction of the total amount of Zn was observed at the organ and cellular levels. This was associated with increased mRNA levels of MT3, Zip3, ZnT4, and ZnT9. MT1–2 gene expression was however repressed during that period. Zip7 and SOD1 were the most abundant transcripts throughout corticogenesis. ZnT10 was included because elevated amounts of ZnT10 proteins were detected at E17. It is proposed that this efflux Zn transporter could play a role in the reduction of the amounts of Zn during corticogenesis

at E17 (end of corticogenesis). Cells of the immature cerebral cortex express a wide diversity of actors involved in the maintenance of Zn homeostasis. Zip7, SOD1, and MTs appeared as the most prominent mRNAs throughout corticogenesis.

Acknowledgements We wish to thank Dr. J. Pérard for his assistance with the ICP-AES experiments and L. Macari for her help with the cell cultures.

Funding Information The study was supported by a grant from l'Agence Nationale de la Recherche (ANR-16-CE29-0024 to AB). We also wish to acknowledge the support from the Centre National de la Recherche Scientifique (CNRS), the Commissariat à l'Energie Atomique et aux Energies Alternatives (CEA), the Université de Grenoble Alpes (UGA), and the France Génomique infrastructure, funded as part of the "Investissements d'Avenir" program managed by the Agence Nationale de la Recherche (contract ANR-10-INBS-09).

Compliance with Ethical Standards

The experimental protocol was approved by the ethical committee of the CEA's Life Sciences Division (CETEA, # A14-006).

Conflict of Interest The authors declare that they have no conflict of interest.

References

1. Finlay BL, Uchiyama R (2015) Developmental mechanisms channeling cortical evolution. Trends Neurosci 38(2):69–76. https://doi.org/10.1016/j.tins.2014.11.004
2. Gotz M, Huttner WB (2005) The cell biology of neurogenesis. Nat Rev Mol Cell Biol 6(10):777–788. https://doi.org/10.1038/nrm1739
3. Takahashi T, Nowakowski RS, Caviness VS, Jr. (1996) The leaving or Q fraction of the murine cerebral proliferative epithelium: a general model of neocortical neuronogenesis. J Neurosci 16 (19):6183–6196
4. Sensi SL, Paoletti P, Bush AI, Sekler I (2009) Zinc in the physiology and pathology of the CNS. Nat Rev Neurosci 10(11):780–791
5. Frederickson CJ, Suh SW, Silva D, Thompson RB (2000) Importance of zinc in the central nervous system: the zinc-containing neuron. J Nutr 130(5S Suppl):1471S–1483S
6. Paoletti P, Vergnano AM, Barbour B, Casado M (2009) Zinc at glutamatergic synapses. Neuroscience 158(1):126–136
7. Barr CA, Burdette SC (2017) The zinc paradigm for metalloneurochemistry. Essays Biochem 61(2):225–235. https://doi.org/10.1042/EBC20160073
8. Takeda A, Tamano H (2017) The impact of synaptic Zn(2+) dynamics on cognition and its decline. Int J Mol Sci 18(11):2411. https://doi.org/10.3390/ijms18112411
9. Vergnano AM, Rebola N, Savtchenko LP, Pinheiro PS, Casado M, Kieffer BL, Rusakov DA, Mulle C et al (2014) Zinc dynamics and action at excitatory synapses. Neuron 82(5):1101–1114. https://doi.org/10.1016/j.neuron.2014.04.034
10. Aizenman E, Stout AK, Hartnett KA, Dineley KE, McLaughlin B, Reynolds IJ (2000) Induction of neuronal apoptosis by thiol oxidation: putative role of intracellular zinc release. J Neurochem 75(5):1878–1888
11. Sensi SL, Ton-That D, Weiss JH (2002) Mitochondrial sequestration and Ca(2+)-dependent release of cytosolic Zn(2+) loads in cortical neurons. Neurobiol Dis 10(2):100–108
12. Sun T, Hevner RF (2014) Growth and folding of the mammalian cerebral cortex: from molecules to malformations. Nat Rev Neurosci 15(4):217–232. https://doi.org/10.1038/nrn3707
13. Jourdren L, Bernard M, Dillies MA, Le Crom S (2012) Eoulsan: a cloud computing-based framework facilitating high throughput sequencing analyses. Bioinformatics 28(11):1542–1543. https://doi.org/10.1093/bioinformatics/bts165
14. Dobin A, Davis CA, Schlesinger F, Drenkow J, Zaleski C, Jha S, Batut P, Chaisson M et al (2013) STAR: ultrafast universal RNA-seq aligner. Bioinformatics 29(1):15–21. https://doi.org/10.1093/bioinformatics/bts635
15. Li H, Handsaker B, Wysoker A, Fennell T, Ruan J, Homer N, Marth G, Abecasis G et al (2009) The sequence alignment/map format and SAMtools. Bioinformatics 25(16):2078–2079. https://doi.org/10.1093/bioinformatics/btp352
16. Anders S, Pyl PT, Huber W (2015) HTSeq–a Python framework to work with high-throughput sequencing data. Bioinformatics 31(2):166–169. https://doi.org/10.1093/bioinformatics/btu638
17. Love MI, Huber W, Anders S (2014) Moderated estimation of fold change and dispersion for RNA-seq data with DESeq2. Genome Biol 15(12):550. https://doi.org/10.1186/s13059-014-0550-8
18. Gibon J, Deloulme J-C, Chevallier T, Ladevèze E, Abrous DN, Bouron A (2013) The antidepressant hyperforin increases the phosphorylation of CREB and the expression of TrkB in a tissue-specific manner. Int J Neuropsychopharmacol 16(1):189–198. https://doi.org/10.1017/S146114571100188X
19. Gee KR, Zhou ZL, Ton-That D, Sensi SL, Weiss JH (2002) Measuring zinc in living cells. A new generation of sensitive and selective fluorescent probes. Cell Calcium 31(5):245–251
20. Tu P, Gibon J, Bouron A (2010) The TRPC6 channel activator hyperforin induces the release of zinc and calcium from mitochondria. J Neurochem 112:204–213
21. Gibon J, Tu P, Bohic S, Richaud P, Arnaud J, Zhu M, Boulay G, Bouron A (2011) The over-expression of TRPC6 channels in HEK-293 cells favours the intracellular accumulation of zinc. Biochim Biophys Acta 1808(12):2807–2818
22. Kiedrowski L (2011) Cytosolic zinc release and clearance in hippocampal neurons exposed to glutamate–the role of pH and sodium. J Neurochem 117(2):231–243. https://doi.org/10.1111/j.1471-4159.2011.07194.x
23. De Samber B, Meul E, Laforce B, De Paepe B, Smet J, De Bruyne M, De Rycke R, Bohic S et al (2018) Nanoscopic X-ray fluorescence imaging and quantification of intracellular key-elements in cryofrozen Friedreich's ataxia fibroblasts. PLoS One 13(1):e0190495. https://doi.org/10.1371/journal.pone.0190495
24. Carmona A, Zogzas CE, Roudeau S, Porcaro F, Garrevoet J, Spiers KM, Salome M, Cloetens P et al (2018) SLC30A10 mutation involved in parkinsonism results in manganese accumulation within nanovesicles of the Golgi apparatus. ACS Chem Neurosci 10:599–609. https://doi.org/10.1021/acschemneuro.8b00451
25. Colvin RA, Jin Q, Lai B, Kiedrowski L (2016) Visualizing metal content and intracellular distribution in primary hippocampal neurons with synchrotron X-ray fluorescence. PLoS One 11(7):e0159582. https://doi.org/10.1371/journal.pone.0159582
26. Colvin RA, Lai B, Holmes WR, Lee D (2015) Understanding metal homeostasis in primary cultured neurons. Studies using single neuron subcellular and quantitative metallomics. Metallomics 7(7):1111–1123. https://doi.org/10.1039/c5mt00084j
27. Pearce LL, Gandley RE, Han W, Wasserloos K, Stitt M, Kanai AJ, McLaughlin MK, Pitt BR et al (2000) Role of metallothionein in nitric oxide signaling as revealed by a green fluorescent fusion protein. Proc Natl Acad Sci U S A 97(1):477–482

28. Sensi SL, Ton-That D, Sullivan PG, Jonas EA, Gee KR, Kaczmarek LK, Weiss JH (2003) Modulation of mitochondrial function by endogenous Zn2+ pools. Proc Natl Acad Sci U S A 100(10): 6157–6162
29. Wagner GP, Kin K, Lynch VJ (2012) Measurement of mRNA abundance using RNA-seq data: RPKM measure is inconsistent among samples. Theory Biosci 131(4):281–285. https://doi.org/10.1007/s12064-012-0162-3
30. Wagner GP, Kin K, Lynch VJ (2013) A model based criterion for gene expression calls using RNA-seq data. Theory Biosci 132(3): 159–164. https://doi.org/10.1007/s12064-013-0178-3
31. Cousins RJ, Liuzzi JP, Lichten LA (2006) Mammalian zinc transport, trafficking, and signals. J Biol Chem 281(34):24085–24089
32. Kambe T, Matsunaga M, Takeda TA (2017) Understanding the contribution of zinc transporters in the function of the early secretory pathway. Int J Mol Sci 18(10). https://doi.org/10.3390/ijms18102179
33. Kambe T, Tsuji T, Hashimoto A, Itsumura N (2015) The physiological, biochemical, and molecular roles of zinc transporters in zinc homeostasis and metabolism. Physiol Rev 95(3):749–784. https://doi.org/10.1152/physrev.00035.2014
34. Juarez-Rebollar D, Rios C, Nava-Ruiz C, Mendez-Armenta M (2017) Metallothionein in brain disorders. Oxidative Med Cell Longev 2017:5828056. https://doi.org/10.1155/2017/5828056
35. Homma K, Fujisawa T, Tsuburaya N, Yamaguchi N, Kadowaki H, Takeda K, Nishitoh H, Matsuzawa A et al (2013) SOD1 as a molecular switch for initiating the homeostatic ER stress response under zinc deficiency. Mol Cell 52(1):75–86. https://doi.org/10.1016/j.molcel.2013.08.038
36. Hershfinkel M (2018) The zinc sensing receptor, ZnR/GPR39, in health and disease. Int J Mol Sci 19(2). https://doi.org/10.3390/ijms19020439
37. Bosomworth HJ, Thornton JK, Coneyworth LJ, Ford D, Valentine RA (2012) Efflux function, tissue-specific expression and intracellular trafficking of the Zn transporter ZnT10 indicate roles in adult Zn homeostasis. Metallomics 4(8):771–779. https://doi.org/10.1039/c2mt20088k
38. Nitzan YB, Sekler I, Hershfinkel M, Moran A, Silverman WF (2002) Postnatal regulation of ZnT-1 expression in the mouse brain. Brain Res Dev Brain Res 137(2):149–157
39. Hartl D, Irmler M, Romer I, Mader MT, Mao L, Zabel C, de Angelis MH, Beckers J et al (2008) Transcriptome and proteome analysis of early embryonic mouse brain development. Proteomics 8(6):1257–1265. https://doi.org/10.1002/pmic.200700724
40. Perez Y, Shorer Z, Liani-Leibson K, Chabosseau P, Kadir R, Volodarsky M, Halperin D, Barber-Zucker S et al (2017) SLC30A9 mutation affecting intracellular zinc homeostasis causes a novel cerebro-renal syndrome. Brain J Neurol 140:928–939. https://doi.org/10.1093/brain/awx013
41. Palmiter RD, Cole TB, Quaife CJ, Findley SD (1996) ZnT-3, a putative transporter of zinc into synaptic vesicles. Proc Natl Acad Sci U S A 93(25):14934–14939
42. Nitzan YB, Sekler I, Silverman WF (2004) Histochemical and histofluorescence tracing of chelatable zinc in the developing mouse. J Histochem Cytochem : Off J Histochem Soc 52(4):529–539. https://doi.org/10.1177/002215540405200411
43. Czupryn A, Skangiel-Kramska J (1997) Distribution of synaptic zinc in the developing mouse somatosensory barrel cortex. J Comp Neurol 386(4):652–660
44. Dufner-Beattie J, Huang ZL, Geiser J, Xu W, Andrews GK (2005) Generation and characterization of mice lacking the zinc uptake transporter ZIP3. Mol Cell Biol 25(13):5607–5615. https://doi.org/10.1128/MCB.25.13.5607-5615.2005
45. Nishikawa M, Mori H, Hara M (2017) Analysis of ZIP (Zrt-, Irt-related protein) transporter gene expression in murine neural stem/progenitor cells. Environ Toxicol Pharmacol 53:81–88. https://doi.org/10.1016/j.etap.2017.05.008
46. Hogstrand C, Kille P, Nicholson RI, Taylor KM (2009) Zinc transporters and cancer: a potential role for ZIP7 as a hub for tyrosine kinase activation. Trends Mol Med 15(3):101–111. https://doi.org/10.1016/j.molmed.2009.01.004
47. Grubman A, Lidgerwood GE, Duncan C, Bica L, Tan JL, Parker SJ, Caragounis A, Meyerowitz J et al (2014) Deregulation of subcellular biometal homeostasis through loss of the metal transporter, Zip7, in a childhood neurodegenerative disorder. Acta Neuropathol Commun 2:25. https://doi.org/10.1186/2051-5960-2-25
48. Chowanadisai W, Graham DM, Keen CL, Rucker RB, Messerli MA (2013) Neurulation and neurite extension require the zinc transporter ZIP12 (slc39a12). Proc Natl Acad Sci U S A 110(24): 9903–9908. https://doi.org/10.1073/pnas.1222142110
49. Lee SJ, Koh JY (2010) Roles of zinc and metallothionein-3 in oxidative stress-induced lysosomal dysfunction, cell death, and autophagy in neurons and astrocytes. Mol Brain 3(1):30. https://doi.org/10.1186/1756-6606-3-30
50. Gunes C, Heuchel R, Georgiev O, Muller KH, Lichtlen P, Bluthmann H, Marino S, Aguzzi A et al (1998) Embryonic lethality and liver degeneration in mice lacking the metal-responsive transcriptional activator MTF-1. EMBO J 17(10):2846–2854. https://doi.org/10.1093/emboj/17.10.2846
51. Pardo CA, Xu Z, Borchelt DR, Price DL, Sisodia SS, Cleveland DW (1995) Superoxide dismutase is an abundant component in cell bodies, dendrites, and axons of motor neurons and in a subset of other neurons. Proc Natl Acad Sci U S A 92(4):954–958
52. Bouron A, Oberwinkler J (2014) Contribution of calcium-conducting channels to the transport of zinc ions. Pflugers Arch 466(3):381–387. https://doi.org/10.1007/s00424-013-1295-z
53. Bouron A, Altafaj X, Boisseau S, De Waard M (2005) A store-operated Ca2+ influx activated in response to the depletion of thapsigargin-sensitive Ca2+ stores is developmentally regulated in embryonic cortical neurons from mice. Brain Res Dev Brain Res 159(1):64–71